Interacting dimer rows on terraces: Reconstructed Si(001) surfaces

R. A. Budiman*
Department of Mechanical and Manufacturing Engineering, University of Calgary, Calgary, Alberta, Canada T2N 1N4
(Received 13 May 2005; published 13 July 2005)

A finite sum of dimer-row elastic interactions on a two-dimensional surface yields a logarithmic stress-domain interaction energy. Using dimer rows as the building blocks of a reconstructed surface generalizes the Alerhand *et al.* and Marchenko models of the stress-domain interaction. Our model is applied to step-height transition on vicinal Si(001) surfaces. The double-layer step phase is determined to be more stable than the single-layer step phase for typical temperatures and miscut angles. A sizable mixed phase region on the temperature-versus-miscut-angle phase diagram is found. The onset of the mixed phase region decreases to a 0° miscut angle if the density of forced kinks is zero. Formation energies of two step types in the Si(001) are positive and consistent with total energy calculations. Our results suggest that the single-layer step phase is stable only for flat Si(001) surfaces.

DOI: 10.1103/PhysRevB.72.035322 PACS number(s): 68.35.Md, 64.70.−p, 68.35.Bs

I. INTRODUCTION

Dimers have been used as elementary building blocks of a reconstructed Si(001) surface in order to understand its thermodynamics.[1] Regarding the dimers as such is reasonable since the surface reconstruction is triggered by a dimerization of surface atoms along the ⟨110⟩ directions,[2,3] creating different surface stresses in the directions parallel and perpendicular to dimer bonds.[4] These anisotropic stress domains formed by dimers occupy terraces punctuated by an array of steps. The number density of the step array is crystallographically (kinematically) imposed when a cutting of the bulk Si crystal is done with a polar miscut angle (miscut angle) toward the [110] axis. There are two types of steps on Si(001): single-layer (SL) steps (each having a single-atomic-layer height) and double-layer (DL) steps. Each step type has two subcategories: S_A and S_B steps for the SL steps, and D_A and D_B steps for the DL steps.[5] For the SL phase—defined as a vicinal Si(001) populated by SL steps—both subcategories are required and alternate since there are two sublattices: 1×2 and 2×1 reconstruction domains. Only D_B steps are required for the DL phase.[5] The forced kink density along the propagation direction of each step depends on the azimuthal miscut angle (tilt angle) toward either the [100] or [010] axis, away from the [110] axis.[6]

Low-energy electron diffraction (LEED) experiments have demonstrated that steps on vicinal Si(001) surfaces with miscut angles 2°–11° are predominantly double layer when annealed at 600–1200 °C.[6–9] The stability of the DL phase is explained by the lower formation energy of two DL steps compared to that of S_A+S_B steps.[5] This was the prevailing idea in understanding the step-height (reconstruction) transition in Si(001) until Alerhand and co-workers[10] proposed a model based on a logarithmic stress-domain interaction for the SL steps.[4] The Alerhand *et al.* model allows for a first-order transition between the SL and DL phases and predicts that the SL phase is the high-temperature phase at a specified miscut angle. A modification to the Alerhand *et al.* model incorporating forced kinks does not change this qualitative behavior.[11] This prediction, however, contradicts the conclusion gathered from the LEED experiments: that the DL phase is more stable at high temperatures.

Another set of experiments using reflection high-energy electron diffraction (RHEED), LEED, and scanning tunneling microscopy[12–15] (STM) report that both SL and DL steps exist at low miscut angles. Especially interesting is the use of a curved substrate to cover a miscut angle range of 0°–5°.[13] The presence of both domains signals an equilibrium between SL and DL phases, which is gradually reduced as the miscut angle increases. Essentially only the DL phase remains when the miscut angle exceeds 6°. It is striking that this behavior is almost independent of temperature.[13] This behavior has been partially explained by a $T=0$ K step-height transition model[16] producing the devil's staircase pattern.[17] A tie-line construction to the free energies of SL and DL phases suggests that a phase equilibrium exists.[18] An extension to the $T=0$ K model[19] correctly identifies the DL phase as a high-temperature phase and finds a critical temperature of 490 K. The authors suggest that the critical temperature may be higher to explain the experimental results.

It has been determined that a step-step interaction[20] plays a negligible role in the stability of DL and SL phases.[4,11,16] The disagreement between the Alerhand *et al.* model and the experiments cannot be attributed to the absence of dipolar step-step interaction in the analysis. The most dominant energy for reconstructed Si(001) comes from the logarithmic stress-domain energy proposed by Alerhand *et al.*[4] and Marchenko.[21] This elastic energy has been cast as an interaction energy between two neighboring terraces, originating from the stress discontinuity as the surface stress changes from one terrace to the next due to the anisotropy. In their derivations, the terraces are assumed structureless and have constant stresses. Since the anisotropic surface stresses of the SL phase rotate 90° from one terrace to the next, it has been postulated that the stress-domain energy for the SL phase is nonzero. Although terraces with DL steps have anisotropic stress-domain terraces, the surface lattice of the DL phase is called "primitive" since all atoms on all terraces belong to a single sublattice.[7] For this reason, the transition between SL and DL phases has been studied[1] by assuming that the stress-domain energy for the DL phase is zero.

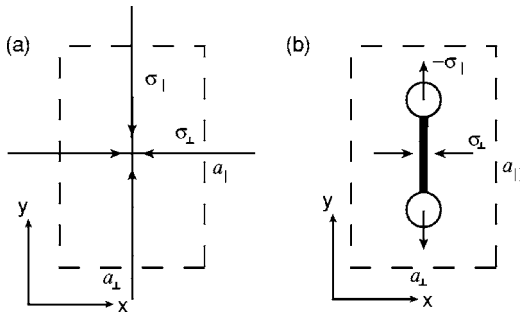

FIG. 1. Two orthogonal line dipoles shown in the left may represent surface stresses of a dimer.

This stark contrast between SL and DL step types hides the fact that both types are constructed from the same dimers. After all, the anisotropic surface stresses originate from two orthogonal stresses of a dimer. In this paper, we show that the logarithmic stress-domain energy can be derived by regarding dimer rows as the elementary building blocks of Si(001). The dimer-row formulation built by striped line dipoles approximates interacting individual dimers. This approach generalizes the earlier derivations by Alerhand *et al.* and Marchenko and endows reconstructed terraces with more microscopic features. The logarithmic stress-domain energy is thus basically a finite sum of dipole-dipole elastic interactions, which model dimer-dimer interactions. The elastic field of a dimer row is identical to that of a step, and hence the offered derivation paints a clearer picture of why a step-step interaction is much weaker than the logarithmic stress-domain energy in the case of reconstructed surfaces. We also show that the critical temperature is significantly higher than 490 K.

Section II starts with obtaining the elastic field of a dimer built by intersecting line dipoles using an elastic Green's function approach. The elastic energy of an isolated two-dimensional terrace composed of arrays of dimers is computed, followed by obtaining the interaction energy between a terrace and its two nearest-neighbor terraces. The resulting internal energy per unit step length is used to compute partition functions for the SL and DL phases. Section III computes the Helmholtz and Gibbs free energies to compare their results. We find the DL phase has a lower free energy within $T=300-1000$ K and a miscut angle range 0°–6°. A phase equilibrium curve obtained from the equal-pressure condition at around 6° is lowered to around 3.5° when the equal chemical-potential condition is used. Section IV compares our results with published results and shows also that the phase equilibrium region depends on the density of forced kinks.

II. STRIPED DIPOLE ARRAYS

Consider a surface unit cell of area $a_\perp a_\parallel$ containing two orthogonal force dipoles as shown in Fig. 1(a). The surface stress along the x axis is $\sigma_\perp$, while the surface stress along the y axis is $\sigma_\parallel$, so that this dipole pair centered at (x_i,y_i) can be written as

$$f_x = \sigma_\perp a_\perp \delta'(x-x_i), \tag{1}$$

$$f_y = \sigma_\parallel a_\parallel \delta'(y-y_i), \tag{2}$$

where $\sigma_\perp$ is aligned along the x axis and $\sigma_\parallel$ along the y axis. The force dipoles above are line dipoles along the x and y axes, intersecting at (x_i,y_i), and are to represent surface stresses caused by dimerization of two surface atoms as shown in Fig. 1(b) by changing the sign of $\sigma_\parallel$. These line dipoles approximate a more complicated expression for surface stresses of an isolated dimer. One consequence of using the line dipoles is that the elastic energy does not include diagonal interactions of dimers. The surface elastic Green's functions $G_{ij}(x,y,z=0)$, where $i,j=x,y$, are[22]

$$G_{xx} = \frac{1+\nu}{\pi E}\left(\frac{1-\nu}{r}+\frac{\nu x^2}{r^3}\right),$$

$$G_{xy} = \frac{\nu(1+\nu)}{\pi E}\frac{xy}{r^3} = G_{yx},$$

$$G_{yy} = \frac{1+\nu}{\pi E}\left(\frac{1-\nu}{r}+\frac{\nu y^2}{r^3}\right),$$

so that the elastic displacements u_i can be computed using

$$u_i = \iint G_{ik}(x-x',y-y')F_k(x',y')dx'dy', \tag{3}$$

giving

$$u_x = -\frac{2\sigma_\perp a_\perp(1-\nu^2)}{\pi E(x-x_i)}, \tag{4}$$

$$u_y = -\frac{2\sigma_\parallel a_\parallel(1-\nu^2)}{\pi E(y-y_i)}. \tag{5}$$

Consider a two-dimensional array of dipole pairs arranged in an $(N+1)\times(M+1)$ cubic lattice such that each dipole pair depicted in Fig. 1(a) is located at $(x_i,y_i)=(na_\perp,ma_\parallel)$, where $n=0,1,\ldots,N$ and $m=0,1,\ldots,M$. We will call this collection of dipole pairs a terrace of size $(N+1)(M+1)$. The total displacement vector is

$$\mathbf{u} = (u_x,u_y) = \frac{2(1-\nu^2)}{\pi E}\left(\sum_{n=0}^{N} -\frac{\sigma_\perp a_\perp}{x-na_\perp}, \sum_{m=0}^{M} -\frac{\sigma_\parallel a_\parallel}{y-ma_\parallel}\right). \tag{6}$$

Accompanying $\mathbf{u}$ is of course the force vector $\mathbf{f}$:

$$\mathbf{f} = (f_x,f_y) = \left(\sum_{n=0}^{N}\sigma_\perp a_\perp \delta'(x-na_\perp), \sum_{m=0}^{M}\sigma_\parallel a_\parallel \delta'(y-ma_\parallel)\right), \tag{7}$$

so that the work done by the dipole array is equal to

$$W = \iint \mathbf{f}\cdot\mathbf{u}\, dx\, dy = -\frac{2\sigma_\perp^2(1-\nu^2)a_\parallel M}{\pi E}\sum_{n<n'}\frac{1}{(n'-n)^2} - \frac{2\sigma_\parallel^2(1-\nu^2)a_\perp N}{\pi E}\sum_{m<m'}\frac{1}{(m'-m)^2}. \quad (8)$$

W represents an interaction energy of dimer rows. The summation $\Sigma_{n<n'}$ does not include terms from $n=n'$ and thus has exactly $(N^2+N)/2$ terms corresponding to the number of combinations when pairing two distinct dimer rows within the set $\{0,1,\ldots,N\}$. This means the summation can be expressed as

$$\sum_{n<n'}\frac{1}{(n-n')^2} = 1\frac{1}{N^2} + 2\frac{1}{(N-1)^2} + \cdots + (N-1)\frac{1}{2^2} + N\frac{1}{1^2} = \sum_{n=0}^{N}\frac{n}{(N+1-n)^2} = \frac{1}{6}\{(N+1)\pi^2 - 6\gamma\} - \psi_0(N+1) - (N+1)\psi_1(N+1), \quad (9)$$

where $\gamma\approx 0.5772$ is Euler's constant and $\psi_n(z)$ the polygamma function of order n, which is the nth derivative of the logarithmic derivative of the gamma function $\Gamma(z)$:

$$\psi_n(z) = \frac{d^n}{dz^n}\frac{\Gamma'(z)}{\Gamma(z)}.$$

A similar result can be obtained for $\Sigma_{m<m'}(m'-m)^{-2}$.

Physically, there is a finite energy for $n=n'$ corresponding to a dimer formation, which is assumed to be a constant α for each dipole pair. Since the elastic work W increases the internal energy E, then the total internal energy for the isolated terrace is

$$E^I = \alpha(N+1)(M+1) - \frac{2\sigma_\perp^{I\,2}a_\parallel(1-\nu^2)M}{\pi E}\left[(N+1)\frac{\pi^2}{6} - \gamma - \psi_0(N+1) - (N+1)\psi_1(N+1)\right] - \frac{2\sigma_\parallel^{I2}a_\perp(1-\nu^2)N}{\pi E}\left[(M+1)\frac{\pi^2}{6} - \gamma - \psi_0(M+1) - (M+1)\psi_1(M+1)\right], \quad (10)$$

where the superscript I is added as we call the terrace that gives Eq. (10) type I. Our zero internal energy corresponds to the absence of dipole pairs on the surface. The fact that the dipole pairs spontaneously form implies that the formation energy $\alpha<0$, while the elastic energy introduced by the elastic field of the dipoles is positive when the work is done to the solid. The type-II terrace is designated as the terrace whose dipole pair orientations are rotated 90° with respect to those of the type-I terrace. For a type-II terrace, $\sigma_\parallel$ is aligned along the x axis, while $\sigma_\perp$ is aligned the y axis. The elastic energy of a type-II terrace of size $(P+1)(M+1)$ is thus

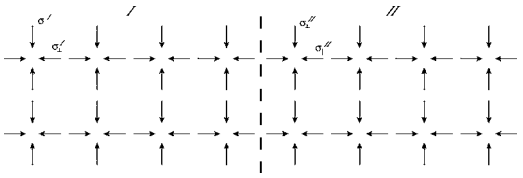

FIG. 2. A domain wall (dashed lines) along the y axis separates type-I and -II terraces. The I-II striped pattern is repeated to fill up the two-dimensional surface. The square symmetry of the dimer arrays requires that $a_\parallel = a_\perp = a$.

$$E^{II} = \alpha(P+1)(M+1) - \frac{2\sigma_\perp^{II^2}a_\parallel(1-\nu^2)P}{\pi E}\left[(M+1)\frac{\pi^2}{6} - \gamma - \psi_0(M+1) - (M+1)\psi_1(M+1)\right] - \frac{2\sigma_\parallel^{II^2}a_\perp(1-\nu^2)M}{\pi E}\left[(P+1)\frac{\pi^2}{6} - \gamma - \psi_0(P+1) - (P+1)\psi_1(P+1)\right]. \quad (11)$$

We place the two terrace types so as to have an alternating I-II pattern that fills up the entire surface. The first domain wall type separates a type-I from a type-II terrace as shown in Fig. 2; the other type is when the type-II terrace precedes the type I. By symmetry, the formation energies for both domain wall types should be identical. There will be interactions between these terraces. We limit the calculation of interaction energy to nearest-neighbor terraces and assume that $a=a_\parallel=a_\perp$. The interaction between a type-I terrace of size $(N+1)(M+1)$ with its two adjacent type-II terraces, each of size $(P+1)(M+1)$, occurs along the x direction. The type-I terrace occupies $0\leqslant x\leqslant Na$, so that the displacement u_x from the type-II terraces is

$$u_x^{II} = -\frac{2(1-\nu^2)\sigma_\parallel^{II}a}{\pi E}\left(\sum_{p=-P-1}^{-1}\frac{1}{x-pa} + \sum_{p=N+1}^{N+P+1}\frac{1}{x-pa}\right). \quad (12)$$

The total force to compute the interaction energy comes from the type-I terrace,

$$f_x^I = \sum_{n=0}^{N}\sigma_\perp^I a\,\delta'(x-na), \quad (13)$$

so that the interaction energy is

$$E_{\text{int}}^I = \iint f_x^I u_x^{II}\, dx\, dy = -\frac{4\sigma_\perp^I\sigma_\parallel^{II}(1-\nu^2)aM}{\pi E}\sum_{n=0}^{N}\{\psi_1(N+1-n) - \psi_1(N+P+2-n)\}. \quad (14)$$

A similar procedure can be applied to the interaction between the type-II terrace and its two nearest-neighboring type-I terraces, giving an interaction energy

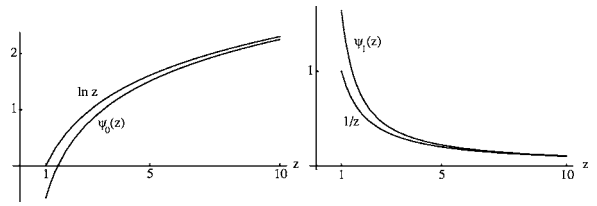

FIG. 3. Plots of $\psi_0(z)$ and $\psi_1(z)$ and their approximations.

$$E_{\text{int}}^{II} = -\frac{4\sigma_{\parallel}^{II}\sigma_{\perp}^{I}(1-\nu^2)aM}{\pi E}\sum_{p=0}^{P}\{\psi_1(P+1-p)-\psi_1(N+P+2-p)\}. \tag{15}$$

The translational unit cell for the infinite striped I-II pattern is two terraces, each of type I and II. The interaction energy for the unit cell is

$$E_{\text{int}} = \frac{1}{2}(E_{\text{int}}^{I}+E_{\text{int}}^{II}),$$

so that the total energy per unit cell is

$$E = E^{I}+E^{II}+E_{\text{int}}. \tag{16}$$

Since the interaction only occurs along the x axis, we can define the energy per unit domain wall length along the y axis:

$$\mathcal{E} = \lim_{M\to\infty} E/aM. \tag{17}$$

We consider sufficiently large N and P so that approximations to the polygamma functions can be used. The Appendix contains approximations used to simplify $\mathcal{E}$, giving

$$\begin{aligned}\mathcal{E} = {} & \frac{2\sigma_{\perp}^{I\,2}(1-\nu^2)}{\pi E}(1+\gamma)-\frac{2\sigma_{\perp}^{I}\sigma_{\parallel}^{II}(1-\nu^2)}{\pi E}\left(\frac{\pi^2}{12}+\gamma\right)\\ & +\frac{2\sigma_{\parallel}^{II2}(1-\nu^2)}{\pi E}(1+\gamma)-\frac{2\sigma_{\perp}^{I}\sigma_{\parallel}^{II}(1-\nu^2)}{\pi E}\left(\frac{\pi^2}{12}+\gamma\right)+\alpha(N\\ & +P+2)-\frac{2\sigma_{\perp}^{I\,2}(1-\nu^2)}{\pi E}\left[\frac{\pi^2}{6}(N+1)-\ln(N+1)\right]\\ & -\frac{2\sigma_{\parallel}^{I2}(1-\nu^2)}{\pi E}\frac{\pi^2}{6}N-\frac{2\sigma_{\parallel}^{II2}(1-\nu^2)}{\pi E}\left[\frac{\pi^2}{6}(P+1)-\ln(P\right.\\ & \left.+1)\right]-\frac{2\sigma_{\perp}^{II\,2}(1-\nu^2)}{\pi E}\frac{\pi^2}{6}P\\ & -\frac{2\sigma_{\perp}^{I}\sigma_{\parallel}^{II}(1-\nu^2)}{\pi E}\ln\frac{(N+1)(N+2)(P+1)(P+2)}{(N+P+2)^2},\end{aligned} \tag{18}$$

by keeping only the linear and logarithmic terms. Figure 3 shows the approximation functions for the polygamma functions; they give a good agreement for N, $P\geqslant 5$.

We can always set the total width of the unit cell equal to L, which may be a constant imposed by kinematics or some other constraints:

$$N+P+2 = L. \tag{19}$$

We can thus rewrite $\mathcal{E}$ by using $\mu = E/2(1+\nu)$, where μ is the shear modulus:

$$\begin{aligned}\mathcal{E} = {} & E_w^{I}+E_w^{II}+\alpha' L+C_4\{2\ln L-\ln[(N+1)(N+2)(L-N-1)\\ & \times(L-N)]\}+C_1(N+1)+C_2\ln(N+1)+C_3\ln(L-N\\ & -1),\end{aligned} \tag{20}$$

where

$$E_w^{I} = \frac{\sigma_{\parallel}^{I^2}\pi(1-\nu)}{6\mu}+\frac{\sigma_{\perp}^{I^2}(1-\nu)}{\pi\mu}(1+\gamma)-\frac{\sigma_{\perp}^{I}\sigma_{\parallel}^{II}(1-\nu)}{\pi\mu}\left(\frac{\pi^2}{12}+\gamma\right),$$

$$E_w^{II} = \frac{\sigma_{\perp}^{II^2}\pi(1-\nu)}{6\mu}+\frac{\sigma_{\parallel}^{II^2}(1-\nu)}{\pi\mu}(1+\gamma)-\frac{\sigma_{\perp}^{I}\sigma_{\parallel}^{II}(1-\nu)}{\pi\mu}\left(\frac{\pi^2}{12}+\gamma\right),$$

$$\alpha' = \alpha-\frac{\pi(1-\nu)}{6\mu}(\sigma_{\perp}^{II^2}+\sigma_{\parallel}^{II^2}),$$

$$C_1 = \frac{\pi(1-\nu)}{6\mu}(\sigma_{\perp}^{II^2}+\sigma_{\parallel}^{II^2}-\sigma_{\perp}^{I^2}-\sigma_{\parallel}^{I^2}),$$

$$C_2 = \frac{\sigma_{\perp}^{I^2}(1-\nu)}{\pi\mu},$$

$$C_3 = \frac{\sigma_{\parallel}^{II^2}(1-\nu)}{\pi\mu},$$

$$C_4 = \frac{\sigma_{\perp}^{I}\sigma_{\parallel}^{II}(1-\nu)}{\pi\mu}.$$

E_w^{I} and E_w^{II} are the domain wall energies, terms in $\mathcal{E}$ that are independent of N and L. The partition function can be computed using

$$\begin{aligned}Z = \sum_N e^{-\beta\mathcal{E}} = {} & e^{-\beta(E_w^{I}+E_w^{II}+\alpha' L)}L^{-2\beta C_4}\sum_N[(N+1)(N+2)\\ & \times(L-N-1)(L-N)]^{\beta C_4}(N+1)^{-\beta C_2}\\ & \times(L-N-1)^{-\beta C_3}e^{-\beta C_1(N+1)},\end{aligned} \tag{21}$$

where $\beta = 1/k_BT$ and k_B is Boltzmann's constant, from which relevant thermodynamic quantities can be derived. The summation sign represents fluctuations of terrace widths, which are physically caused by kinks that are thermally excited and not due to kinematics.

III. RECONSTRUCTED SILICON(001)

There have been many important works, theoretical and experimental, devoted to understanding the reconstructed

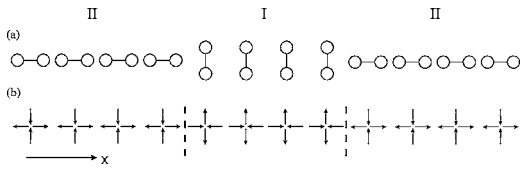

FIG. 4. (a) A band of alternating dimer array along the x axis on a Si(001) surface is modeled by (b) alternating dipole arrays.

Si(001) surfaces.[1,23] One important motivation is the presence of two alternating types of steps (domain walls), S_A and S_B steps, when the Si(001) is mechanically cut with small miscut angles. These alternating steps cause antiphase domains when growing epitaxial layers on top of a Si(001) substrate (Fig. 4). Tong and Bennett[13] observe using microprobe RHEED that S_A steps are spaced regularly, while an S_B step, bounded by two S_A steps on its left and right, meanders. The regular spacing of S_A steps permits us to use the constant total width assumption, i.e., constant $N+P+2=L$.

We use anisotropic surface stresses from total energy calculations for consistency, which are equal in magnitudes ($\sigma = 0.035$ eV/Å^2) but opposite in directions.[4,10] The surface stress along the dimer bond is found to be tensile, while the stress perpendicular to the bond is compressive. Thus, the corresponding anisotropic dimer forces are characterized by the following quantities in our model:

$$\sigma_{\parallel}^{I} = \sigma_{\parallel}^{II} = -\sigma, \quad \sigma_{\perp}^{I} = \sigma_{\perp}^{II} = \sigma, \tag{22}$$

so that the force dipoles parallel to the dimer bonds (i.e., $\propto\sigma_{\parallel}$) are tensile, while the dipoles perpendicular to the dimer bonds ($\propto\sigma_{\perp}$) are compressive. Hence, Eq. (21) becomes

$$Z_s = e^{-\beta(2E_{\rm ws}+\alpha' L)} L^{2\beta C_2} \sum_N [(N+1)^2(N+2)(L-N-1)^2(L-N)]^{-\beta C_2} \tag{23}$$

where $E_w^I = E_w^{II} \approx 1.4712\sigma^2(1-\nu)/\mu \equiv E_{\rm ws}$; $\alpha' = \alpha - \pi\sigma^2(1-\nu)/3\mu$; $C_1=0$; $C_2=C_3=\sigma^2(1-\nu)/\pi\mu$; and $C_4=-C2$. The subscript s is added to indicate that the partition function is for the SL phase that has the alternating S_A and S_B step pattern. To facilitate computation, we assume $N\approx N+1$, $N+2$, so that

$$Z_s \approx e^{-\beta(2E_{\rm ws}+\alpha' L)} L^{2\beta C_2} \sum_{N=1}^{L-1} \frac{1}{[N(L-N)]^{3\beta C_2}}, \tag{24}$$

since the minimum terrace width is 1, while the maximum is $L-1$. Using the Euler summation formula to approximate the summation:

$$Z_s \approx e^{-\beta(2E_{\rm ws}+\alpha' L)} L^{2\beta C_2} \{(L-1)^{-3\beta C_2} + L^{1-6\beta C_2}[B_{1-L^{-1}}(1-3\beta C_2, 1-3\beta C_2) - B_{L^{-1}}(1-3\beta C_2, 1-3\beta C_2)]\}, \tag{25}$$

where $B_m(r,s)$ is the incomplete beta function (see the Appendix). For silicon, $\mu = C_{44} = 0.4969$ eV/Å^3 and $\nu = C_{12}/(C_{11}+C_{12}) = 0.2783$, so that $C_2 = \sigma^2(1-\nu)/\pi\mu = 0.5666$ meV/Å. Thus, $1-3\beta C_2 = 1-3C_2/k_BT \approx 1$ for $T = 300-1000$ K. The approximation to Z_s is tuned in this temperature regime using up to the linear term in the expansion of $B_m(r,s)$ around $r=s=1$,

$$B_m(1-3\beta C_2, 1-3\beta C_2) = m - 3\beta C_2[m\ln m - (1-m)\ln(1-m) - 2m] + \mathcal{O}(9\beta^2 C_2^2).$$

Letting $L\approx L-1$, $L-2$, the partition function simplifies into

$$Z_s \approx e^{-\beta(2E_{\rm ws}+\alpha' L)} L^{-\beta C_2}[1 + L^{1-3\beta C_2}(1+6\beta C_2)] \tag{26}$$

giving a free energy

$$F_s = -\beta^{-1}\ln Z_s = 2E_{\rm ws} + \alpha' L + C_2 \ln L - \beta^{-1}\ln[1 + L^{1-3\beta C_2}(1+6\beta C_2)]. \tag{27}$$

At a sufficiently high temperature, such that $\beta C_2 \ll 1$, the free energy can be approximated by

$$F_s(\beta C_2 \ll 1) = 2E_{\rm ws} + \alpha' L + C_2 \ln L - k_B T \ln[L+1] \approx 2E_{\rm ws} + \alpha' L + (C_2 - k_B T)\ln L, \tag{28}$$

resembling the Alerhand *et al.* model of interacting stress-domain energy,[4] except in this case the coefficient for the ln L term has an entropic contribution. The linear term in L does not appear in their model since they did not consider the dangling bond energy to create a terrace of width L. At $T = 300-1000$ K, $C_2 < k_BT$; thus, the free energy minimization by increasing L is caused by entropy rather than by elastic strain relaxation.

The DL phase corresponds to the presence of a single type of step on the vicinal Si(001) surface. The alternating striped terraces disappear in the D_B phase. It is known also that only type-I terraces survive,[6] so that the dimer forces are characterized by

$$\sigma_{\parallel}^{I} = \sigma_{\perp}^{II} = -\sigma, \quad \sigma_{\perp}^{I} = \sigma_{\parallel}^{II} = \sigma, \tag{29}$$

where the equalities are simply to turn the type-II terrace into a type-I terrace. Hence, the partition function for the D_B phase is

$$Z_d = e^{-\beta(2E_{\rm wd}+\alpha' L)} L^{-2\beta C_2} \sum_{N=1}^{L-1} \frac{1}{[N(L-N)]^{\beta C_2}}, \tag{30}$$

where $E_w^I = E_w^{II} \approx 0.5801\sigma^2(1-\nu)/\mu \equiv E_{\rm wd}$; $C_4 = C_2 = C_3 = \sigma^2(1-\nu)/\pi\mu$; and α' is defined as before. Contrary to the Alerhand *et al.* model,[4,10] where the elastic interaction energy is zero for the DL phase, our model produces a finite logarithmic interaction due to $C_4 \neq 0$ since the interaction is no longer defined by a stress discontinuity at a domain wall but is now given by dipole-dipole interactions. The domain wall energy $E_{\rm wd}$ for the DL phase is about 2.5 times smaller than $E_{\rm ws}$ for the SL phase. When a step occupies the domain wall's position, the wall energy should correspond to the step formation energy minus a formation energy associated with the step's ledge. The approximation for Z_d is obtained using the same method for Z_s:

$$Z_d \approx e^{-\beta(2E_{\rm wd}+\alpha' L)} L^{-3\beta C_2}[1 + L^{1-\beta C_2}(1+2\beta C_2)], \tag{31}$$

producing

$$F_d = 2E_{\mathrm{wd}} + \alpha' L + 3C_2 \ln L - \beta^{-1} \ln[1 + L^{1-\beta C_2}(1 + 2\beta C_2)]. \tag{32}$$

The high-temperature behavior of F_d is similar to that of F_s, where the entropic contribution proportional to β^{-1} overcomes the logarithmic stress-domain term.

The phase boundary between the SL and the DL phases in the case of constant volume aL is determined by $\Delta F = F_s - F_d = 0$, giving

$$2(E_{\mathrm{ws}} - E_{\mathrm{wd}}) - 2C_2 \ln L - \beta^{-1} \ln\left(\frac{1 + L^{1-3\beta C_2}(1 + 6\beta C_2)}{1 + L^{1-\beta C_2}(1 + 2\beta C_2)}\right) = 0. \tag{33}$$

As expected, the phase boundary does not depend on the dimer formation energy α. The more stable phase at a certain T and aL (representing volume) has the lower free energy. In our model, ΔE_w is completely determined from the two elastic constants and the dipole (dimer) force σ. In fact using the parameters $\sigma = 0.035$ eV/Å^2, $\mu = 0.4969$ eV/Å^3, $\nu = 0.2783$, we find $F_d < F_s$ within $T = 300-1000$ K and $L = 1-10\,000$. Hence, the DL phase is more stable than the SL phase for this range. The DL phase remains more stable when σ is decreased from 0.035 eV/Å^2 to close to zero. From these parameters, we also find $E_{\mathrm{ws}} = 0.026$ eV/Å and $E_{\mathrm{wd}} = 0.0010$ eV/Å. Total energy calculations can provide ΔE_w independently from the determination of the other two terms in the phase boundary condition $\Delta F = 0$. For example, the wall formation energy for the single-layer step phase is equal to the sum of formation energies of S_A and S_B steps: $E_{\mathrm{ws}} = 0.020$ eV/Å, while $E_{\mathrm{wd}} = 0.0065$ eV/Å can be computed from the double-layer step formation energy.[5] These two values are consistent with our wall energies above.

A stable SL phase starts to appear at $L \approx 220$ when σ is increased to 0.18 eV/Å^2. Such a large dimer force, however, implies a large deformation of roughly $\sigma/\mu = 0.36$Å and may break the dimer bond. This effect does not occur during the reconstruction transition of vicinal Si(001). The dependence of thermodynamic quantities on the miscut angle θ can obtained using

$$\tan\theta = 2/L, \tag{34}$$

where the constant 2 accounts for the total height per total width L for either two single-layer steps for a unit cell of two terraces (the SL phase), or one double-layer step for a unit cell of single terrace (the DL phase). Thus, $L = 220$ corresponds to a miscut angle of $\theta = 0.52°$ and we can also say that the DL phase is stable down to $\theta = \tan^{-1}(2/10\,000) = 0.011°$.

Despite the absence of a stable SL step phase, it is possible that the SL phase exists and is in equilibrium with the DL phase for typical σ. The presence of a SL phase can be imposed by kinematics of crystal cutting. In this respect, the total width L is regarded as a quenched external field.[24] We have in fact used this condition when previously stating that L is constant. The constant L manifests, for example, in a constant distance between two smooth nearby S_A steps that confine one S_B step. The S_B step can meander between two S_A steps without crossing them. A phase equilibrium is determined by the equal free energy gradient condition, which in this case is given by the equal-"pressure" condition $\Delta P = P_s - P_d = 0$, where

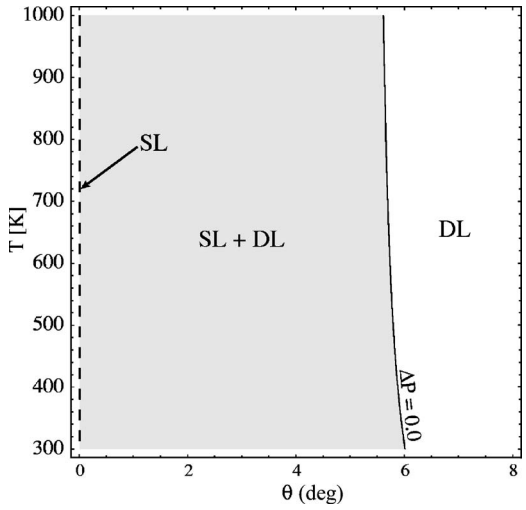

FIG. 5. The θ-T phase diagram assuming constant volume aL, i.e., when L is regarded as quenched (imposed by kinematics). Parameters used are $\sigma = 0.0035$ eV/Å^2, $\mu = 0.4969$ eV/Å^3, $\nu = 0.2783$, and $a = 3.84$ Å. The SL phase is postulated to occur at the $L \to \infty$ limit.

$$P_s = -\frac{\partial F_s}{\partial(aL)} = -\alpha' - \frac{C_2}{L} + \frac{(1 - 3\beta C_2)(1 + 6\beta C_2)}{\beta(L + L^{3\beta C_2} + 6\beta C_2 L)}, \tag{35}$$

$$P_d = -\frac{\partial P_d}{\partial(aL)} = -\alpha' - \frac{3C_2}{L} + \frac{1 + \beta C_2(1 - 2\beta C_2)}{\beta(L + L^{\beta C_2} + 2\beta C_2 L)}. \tag{36}$$

Both pressures obey a thermodynamic inequality $-\partial P_i/\partial L > 0$ over $T = 300-1000$ K and $L = 1-100$, ensuring that each phase is thermodynamically viable. These pressures are basically generalized forces conjugate to the total width L. A phase equilibrium curve ($\Delta P = 0$) is found around $\theta = 6°$ as shown in Fig. 5. It is clear from the expressions of P_i that the phase equilibrium cannot occur solely by elastic forces. A $T = 0$ K model for the phase equilibrium should not be extrapolated to predict a finite-temperature equilibrium. Throughout the temperature and miscut angle ranges of practical interest, we find that the DL phase is more stable than the SL phase, yet we also find a phase equilibrium curve of the two phases at $\theta = 6°$. We thus postulate that the stable SL phase for vicinal Si(001) occurs at the limit $L \to \infty$, i.e., at the flat surface limit. This is motivated by the stability of the DL phase at the $\beta \to 0$ and $L \to \infty$ limits,

$$\lim_{L\to\infty}\lim_{\beta\to 0} \Delta F = 2(E_{\mathrm{ws}} - E_{\mathrm{wd}} - 2C_2) > 0$$

for the Si(001) parameters, so that the phase equilibrium curve will eventually touch the $\theta = 0°$ axis at some temperature greater than 1000 K. The only location left for a stable SL phase is thus along this axis. Figure 5 incorporates this hypothesis. We note that the low-temperature limit ($\beta \to \infty$)

cannot be assessed since the approximations for the partition functions are not good for this limit.

When the constant volume aL is relaxed and the process leading to a lower free energy is thus done at a constant pressure and temperature, the phase equilibrium curve actually moves to a lower miscut angle. Hence, L fluctuations further stabilize the DL phase. In this situation, the grand canonical ensemble should be the appropriate vehicle although such analysis is not performed here. Using this ensemble, the nature of statistical distribution of L, i.e., the terrace width distribution, may become clearer. At any rate, we can at least obtain the chemical potential μ_i by performing the Legendre transformation to the free energy F_i to obtain the Gibbs free energy $\Phi_i = F_i + P_i aL$, where $\mu_i = \partial\Phi_i / \partial L$, since L also acts as the number of particles variable:

$$\mu_s = \frac{\beta C_2 L^{6\beta C_2} - \beta C_2 L^{1+3\beta C_2}(1+6\beta C_2)(1-9\beta C_2) - (1-4\beta C_2)L^2(1+6\beta C_2)^2}{\beta L(L + L^{3\beta C_2} + 6\beta C_2 L)^2}, \tag{37}$$

$$\mu_d = \frac{3\beta C_2 L^{2\beta C_2} + \beta C_2 L^{1+\beta C_2}(5+\beta C_2)(1+2\beta C_2) - (1-4\beta C_2)L^2(1+2\beta C_2)^2}{\beta L(L + L^{\beta C_2} + 2\beta C_2 L)^2}. \tag{38}$$

Both phases are thermodynamically viable as $\partial\mu_s/\partial N > 0$ and $\partial\mu_d/\partial N > 0$ within the temperature and miscut ranges. Figure 6 shows the θ-T phase diagram containing the phase equilibrium formed by $\Delta\mu = \mu_s - \mu_d = 0$. The phase equilibrium curve is now significantly shifted to a lower angle of about 3.5°. This phase diagram also uses the Gibbs free energy difference $\Delta\Phi = \Phi_s - \Phi_d$ to determine the relative stability of the two phases.

We find $\Phi_d < \Phi_s$ throughout the ranges; hence, we find the DL phase to be also more stable than the SL phase when the unit cell width L can fluctuate. Figure 6 explains the Tong and Bennett experiments:[13] it shows that the gradual strength of the DL phase with increasing miscut angle is independent of temperature. The high-temperature limit as $L \to \infty$ is also the DL phase, $\lim_{L\to\infty}\lim_{\beta\to 0}\Delta\Phi = 2(E_{\rm ws} - E_{\rm wd} - 2C_2) > 0$, identical with the result using ΔF, implying that the phase

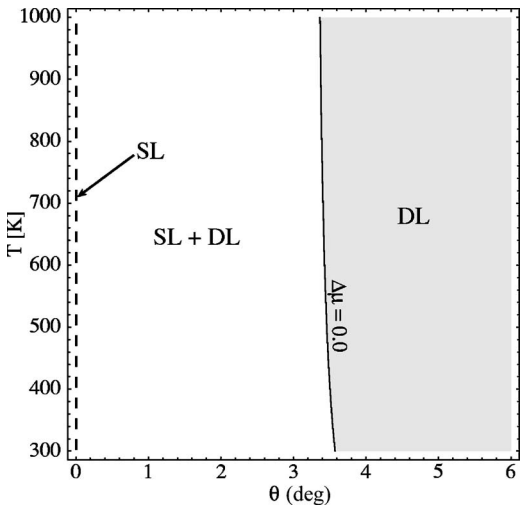

FIG. 6. The θ-T phase diagram constructed using the Gibbs free energy. Same parameters used for Fig. 5 are used here. This phase diagram should be more faithful to experiments than shown in Fig. 5 since fluctuations in L are allowed.

equilibrium curve will touch the $\theta = 0°$ axis at a temperature higher than 1000 K. Comparing the step formation energies $E_{\rm ws}$ and $E_{\rm wd}$ to predict the relative stability of SL and DL phases as done by Chadi[5] is comparable to the evaluation of limits above. There is experimental evidence that SL steps spontaneously form on almost flat Si(001) surfaces.[26] STM studies have also shown that for $\theta < 2°$ the surface displays SL steps.[27]

A surface with a changing L should correspond to a two-terrace unit cell receiving dimers from outside the unit cell. Annealing that transports dimers between two nearby two-terrace unit cells of different widths, say L_j and L_k, can change these widths. These transported dimers may modify the widths of type-I and type-II terrace components of the unit cell. A much clearer example of a variable-L surface is a deposition of dimers on Si(001). It is still possible to have a constant-L surface during annealing, when a step confined by its two terraces meanders without crossing the bounding steps. In Si(001), S_B steps are known to meander while S_A steps remain largely stationary. The constant distance between two neighboring S_A steps is a good approximation, although in real systems the terrace widths can be expected follow a bell distribution. The phase equilibrium defined by $\Delta\mu$ therefore paints a more realistic picture for both annealing and deposition than that by ΔP.

IV. COMPARISONS

The equal-chemical-potential condition $\mu_s = \mu_d$ predicts a phase equilibrium curve at around 3.5°. The phase equilibrium region extends from 0° to 3.5°, prompting us to propose that the SL phase is stable only at the $\theta \to 0°$ limit up to some $T > 1000$ K. Our results agree with the cited experiments, although they disagree with several models using the Alerhand *et al.* model. The fundamental disagreement between our model and the Alerhand *et al.* model is that the Alerhand *et al.* model assumes a zero logarithmic stress-domain interaction for the DL phase,[10,11] while we show that such inter-

action actually exists since dimers interact across terraces. The models lead to different phase diagrams. The Alerhand *et al.* model produces a phase diagram in which the SL phase is more stable than the DL phase at high temperatures, while our phase diagram (Fig. 6) shows that it is the DL phase that is more stable.

The previous disagreement between the Alerhand *et al.* model and most experimental data has led to serious discussions in the literature. One set of discussions is about whether a phase equilibrium region separating stable SL and DL phases exists.[10,18,24] Essentially, the issue is about whether θ is a proper thermodynamic variable. If it is, then there is typically a range of miscut angle values in which SL and DL phases coexist near a first-order transition (phase boundary) curve. The miscut angle θ is kinematically imposed and thus can act like a quenched density.[24] However, experiments have shown clearly that the terrace widths fluctuate in some manner. We show that the kinematic constraint is kept when a canonical ensemble is used. However, a better agreement with experiments should be obtained when the unit cell width L fluctuates in the grand canonical ensemble formulation (not done in this work).

Another set of discussions focuses on whether SL and DL phases can coexist at low miscut angles. Yang *et al.*[15] reported that both step types were observed by scanning tunneling microscopy of 0.5°-miscut Si(001) annealed at 1473 K. This finding was later disputed by Zandvliet[25] who states that the observation by Yang *et al.* disagrees with the Alerhand *et al.* model. When thermal fluctuations, reliable step edge freeze-in temperature, and step formation energies are taken into account, the Alerhand *et al.* model predicts the onset of the phase coexistence at 1.1°. Yang *et al.*[28] replied by confirming their observations and stating that the formation energy of the DL phase is lower than that of the SL phase; hence the SL steps will collapse into the DL steps. This scenario was proposed by Pehlke and Tersoff,[16] who argued that faceting due to a phase equilibrium of SL and DL phases does not happen since the energy can always be lowered every time alternating SL and DL steps can form. At low miscut angles, the alternating S_A and S_B steps imposed by kinematics will prefer this scenario with the resulting step pattern resembling the devil's staircase pattern.[17] Our model shows a phase equilibrium of SL and DL phases at $T=300-1000$ K. Using the lever rule in Fig. 6 the fractional population of the two phases can be computed. Kinematics and a substantial mass transfer requirement would prevent faceting from occurring even though both SL and DL steps are present for low miscut angles.

Our model can numerically produce a phase equilibrium region that does not extend to 0° by adding $\mu_0>0$ to $\Delta\mu=0$:

$$\mu_s - \mu_d = \mu_0. \tag{39}$$

A tiny change in μ_0 changes the phase equilibrium range considerably as shown in Fig. 7, where now the phase equilibrium range is between 0.9° and 3.5° by setting $\mu_0=0.2604\times10^{-7}$ eV/Å. Which physical quantity is represented by μ_0? Our model assumes all steps are straight as shown in the top picture of Fig. 8. When kinks, tilting the step direction at some angle ϕ, are present, shown in the bottom picture of Fig. 8, a constant term should appear in $\Delta\mu$ since $\mu_i=\partial\Phi_i/\partial L$. The constant term accounts for introducing this kink as L changes by one unit length a. These kinks are not included our model and are now introduced to show that they affect the onset of the phase coexistence region.

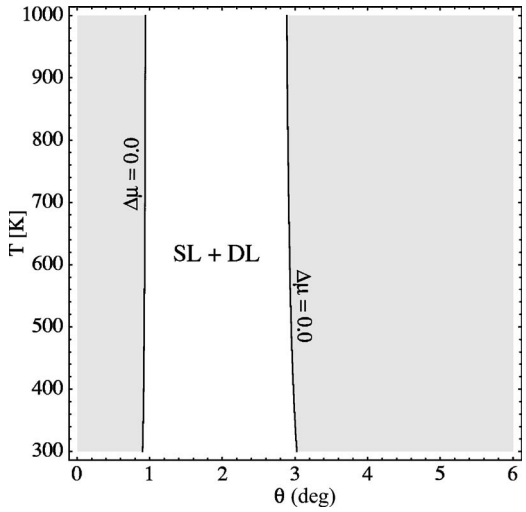

FIG. 7. The θ-T phase diagram with $\mu_s-\mu_d=\mu_0>0$. The phase equilibrium region is now between 0.9° and 3.0° by arbitrarily setting $\mu_0=0.2604\times10^{-7}$ eV/Å. Outside this region, $\mu_s<\mu_d+\mu_0$. μ_0 is shown to be directly proportional to the density of forced kinks. The plot shown corresponds to a tilt angle of 0.5°. Same parameters used for Fig. 5 are used here.

These kinks should correspond to the so-called forced kinks which are produced when the cutting is tilted at some azimuth angle. The forced kinks are geometrical, while thermal kinks are physical fluctuations from adatoms and dimers. The axis of rotation of the tilt angle ϕ is [001], while the axis of rotation for the miscut angle θ is [110]. The tilt angle ϕ is related to the average distance l between two nearby kinks of a step by $\tan\phi=a/l$. The contribution of forced kinks to $\Delta\mu$ is

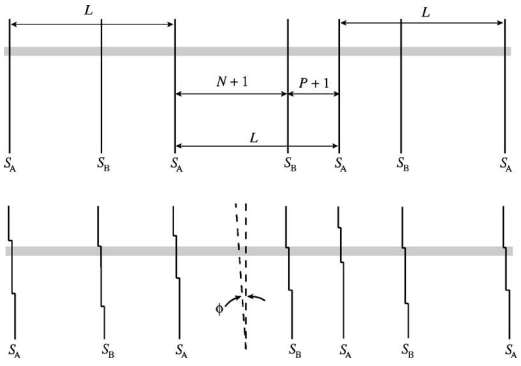

FIG. 8. The top picture shows that all steps are straight so that per unit step length (the gray band) the energetics does not contain contributions from kinks. The bottom picture shows that a constant contribution to the chemical potential, independent of terrace width, will appear when kinks of a unit length due to a tilt angle ϕ are included.

$$\mu_0 = \Delta E_k/(l/a)^2 = \Delta E_k \tan^2\phi,$$

where one factor (l/a) is used to equally divide the forced-kink formation energy difference ΔE_k among (l/a) bands (only one shown in the bottom picture of Fig. 8). The other factor of (l/a) is to recognize that the average kink energy difference $\Delta E_k/(l/a)$ must still be divided by (l/a) since the probability of having a kink for each band is $(l/a)^{-1}$. Since for single-layer steps a kink along an S_A step is a unit length of the S_B step, and vice versa, the forced-kink formation energy difference is equal to

$$\Delta E_k = \frac{1}{2}E_{\rm ws} - E_{\rm wd} = 0.1555\sigma^2(1-\nu)/\mu,$$

where the factor 1/2 is included since the single-layer wall energy $E_{\rm ws}$ does not distinguish the S_A step from the S_B step; each unit cell of width L needs both step types. Hence,

$$\mu_0 = 0.1555\sigma^2(1-\nu)\tan^2\phi/\mu, \tag{40}$$

giving $\mu_0 = 0.2107\times10^{-7}$ eV/Å for $\phi = 0.5°$, which is very close to the set value of 0.2604×10^{-7} eV/Å used to create Fig. 7. Hence, the onset of the phase equilibrium sensitively depends on the density of forced kinks. Figure 7 thus corresponds to a tilt angle of about 0.5°. When $\phi = 0$, the region extends from 0° to 3.5°, and the range is decreased as ϕ is increased. The phase equilibrium disappears for $\mu_0 > 0.52\times10^{-7}$ eV/Å corresponding to $\phi > 0.78°$. Adding μ_0 into $\Delta\mu$ may change the relative stability of the two phases; thus, we do not know whether SL or DL phase is more stable at high tilt angles. The partition functions should incorporate the kink energy to predict their relative stability outside the phase equilibrium region in the presence of forced kinks.

V. CONCLUSIONS

We show that dipole-dipole interactions on a terrace, where each intersecting dipole pair represents a dimer, may lead to a logarithmic stress-domain energy. This approach generalizes the elastic interaction energy between two neighboring terraces proposed by Alerhand *et al.* and Marchenko. It also clarifies the fact that the step-step (dipole-dipole) interaction energy is much weaker than the stress-domain energy in reconstructed surfaces by showing that the stress-domain energy is basically a finite sum of dipole-dipole interaction energy. Fluctuations in terrace widths due to thermal kinks are incorporated in the canonical-ensemble partition functions for the SL and DL phases. The free energy for the DL phase is found lower than that of the SL phase within $T = 300-1000$ K and $\theta = 0°-6°$. A phase equilibrium curve at a large miscut angle of 6° is found. A phase equilibrium for both phases from the Gibbs free energy occurs at a miscut angle of 3.5°. Since terrace widths vary in general, the phase equilibrium curve at 3.5° should be more realistic than that from the equal-pressure condition. The Gibbs free energy of the double-layer step phase is lower as well. The forced-kink density plays a major role in modifying the miscut angle range of the phase equilibrium region.

ACKNOWLEDGMENT

The author acknowledges the financial support of NSERC (Natural Sciences and Engineering Research Council of Canada) through its Discovery Grant.

APPENDIX: APPROXIMATION FORMULAS

Since

$$\psi_0(z) = \frac{d}{dz}\ln\Gamma(z) \approx \ln z - \frac{1}{2z},$$

for large z

$$\psi_0(z) \approx \ln z - \frac{1}{2z},$$

$$\psi_1(z) \approx \frac{1}{z} + \frac{1}{2z^2}.$$

We also use the Euler summation formula (trapezoid rule)

$$\sum_{k=0}^{K} f(k) \approx \frac{1}{2}[f(K)+f(0)] + \int_0^K f(x)dx$$

to approximate, for example,

$$\sum_{n=0}^{N} \psi_1(N+1-n) \approx \frac{1}{2}[\psi_1(1)+\psi_1(N+1)] + \int_0^N \psi_1(N+1-x)dx = \frac{\pi^2}{12} + \gamma + \ln(N+1) + \frac{1}{2(N+1)},$$

where $\gamma \approx 0.5772$ is the Euler constant. The incomplete beta function $B_m(r,s)$ is given by

$$B_m(r,s) = \int_0^m x^{r-1}(1-x)^{s-1}dt.$$

*Electronic address: budiman@enme.ucalgary.ca

[1] H. J. W. Zandvliet, Rev. Mod. Phys. **72**, 593 (2000).
[2] R. E. Schlier and H. E. Farnsworth, J. Chem. Phys. **30**, 917 (1959).
[3] R. M. Tromp, R. J. Hamers, and J. E. Demuth, Phys. Rev. Lett. **55**, 1303 (1985).
[4] O. L. Alerhand, D. Vanderbilt, R. D. Meade, and J. D. Joannopoulos, Phys. Rev. Lett. **61**, 1973 (1988).
[5] D. J. Chadi, Phys. Rev. Lett. **59**, 1691 (1987).
[6] T. Nakayama, Y. Tanishiro, and K. Takayanagi, Jpn. J. Appl. Phys., Part 2 **26**, L280 (1987).
[7] R. Kaplan, Surf. Sci. **93**, 145 (1980).
[8] B. Z. Olshanetsky and V. I. Mashanov, Surf. Sci. **111**, 414 (1981).
[9] R. D. Bringans, R. I. G. Uhrberg, M. A. Olmstead, and R. Z.

Bachrach, Phys. Rev. B **34**, 7447 (1986).
[10] O. L. Alerhand, A. N. Berker, J. D. Joannopoulos, D. Vanderbilt, R. J. Hamers, and J. E. Demuth, Phys. Rev. Lett. **64**, 2406 (1990).
[11] T. W. Poon, S. Yip, P. S. Ho, and F. F. Abraham, Phys. Rev. Lett. **65**, 2161 (1990).
[12] T. Sakamoto and G. Hashiguchi, Jpn. J. Appl. Phys., Part 2 **25**, L78 (1986).
[13] X. Tong and P. A. Bennett, Phys. Rev. Lett. **67**, 101 (1991).
[14] J. J. de Miguel, C. E. Aumann, R. Kariotis, and M. G. Lagally, Phys. Rev. Lett. **67**, 2830 (1991).
[15] H. Q. Yang, C. X. Zhu, J. N. Gao, Z. Q. Xue, and S. J. Pang, Surf. Sci. **429**, L481 (1999).
[16] E. Pehlke and J. Tersoff, Phys. Rev. Lett. **67**, 465 (1991).
[17] P. Bak and R. Bruinsma, Phys. Rev. Lett. **49**, 249 (1982).
[18] N. C. Bartelt, T. L. Einstein, and C. Rottman, Phys. Rev. Lett. **66**, 961 (1991).
[19] E. Pehlke and J. Tersoff, Phys. Rev. Lett. **67**, 1290 (1991).
[20] V. I. Marchenko and A. Ya. Parshin, Sov. Phys. JETP **52**, 129 (1980).
[21] V. I. Marchenko, JETP Lett. **33**, 381 (1981).
[22] L. D. Landau and E. M. Lifshitz, *Theory of Elasticity* (Butterworth-Heinemann, Oxford, 1986), p. 25.
[23] D. Haneman, Rep. Prog. Phys. **50**, 1045 (1987).
[24] O. L. Alerhand, A. Nihat Berker, J. D. Joannopoulos, D. Vanderbilt, R. J. Hamers, and J. E. Demuth, Phys. Rev. Lett. **66**, 962 (1991).
[25] H. J. W. Zandvliet, Surf. Sci. **449**, L263 (2000).
[26] L. Zhong, A. Hojo, Y. Matsushita, Y. Aiba, K. Hayashi, R. Takeda, H. Shirai, H. Saito, J. Matsushita, and J. Yoshikawa, Phys. Rev. B **54**, R2304 (1996).
[27] R. J. Hamers, R. M. Tromp, and J. E. Demuth, Phys. Rev. B **34**, 5343 (1986).
[28] H. Q. Yang, C. X. Zhu, J. N. Gao, Z. Q. Xue, and S. J. Pang, Surf. Sci. **449**, L265 (2000).